AIAA JOURNAL
Vol. 35, No. 1, January 1997

Active Control of Fan-Generated Tone Noise

Carl H. Gerhold*
NASA Langley Research Center, Hampton, Virginia 23681

An experiment to control the noise radiated from the inlet of a ducted fan using a time domain active adaptive system is reported on. The control sound source consists of loudspeakers arranged in a ring around the fan duct. The error sensor location is in the fan duct. The purpose of this experiment is to demonstrate that the in-duct error sensor reduces the mode spillover in the far field, thereby increasing the efficiency of the control system. The control system is found to reduce the blade passage frequency tone significantly in the acoustic far field when the mode orders of the noise source and of the control source are the same, when the dominant wave in the duct is a plane wave. The presence of higher-order modes in the duct reduces the noise reduction efficiency, particularly near the mode cut on where the standing wave component is strong, but the control system converges stably. The control system is also found to be stable and convergent when the first circumferential mode is generated in the duct both by the fan and by the control source. The control system is found to reduce the fan noise in the far field on an arc around the fan inlet by as much as 20 dB with none of the sound amplification associated with mode spillover.

Introduction

THE emergence of the ultra-high bypass ratio engine on aircraft in the 21st century is expected to pose new and significant challenges to the noise control engineers. The dominant engine noise source will shift from the jet to the fan. The blade tip speed will be subsonic or transonic so that the fan noise will have high tonal content at harmonics of the blade passage frequency and the fundamental tone will be at a frequency less than 1000 Hz. To provide sufficient thrust, the engine diameter will be on the order of 3.66 m (12 ft); in fact, engine size will be limited by considerations such as space available under the wing and allowable landing gear length. Weight is a significant parameter in the design of the power plant, and to minimize the weight of the large diameter nacelle, it will be as short and as thin as possible. The relatively low blade passage frequency would necessitate thick bulk liner treatment, which is extensive in the axial direction, while thickness and length restrictions limit the amount of passive noise control treatment that can be applied.

The conflicting goals of minimum weight and maximum noise reduction can be aided materially by active noise control. Active noise control is well suited for applications in which a low-frequency noise source limits the utility of passive control methods.[1] An active noise control system can provide significant noise reduction without excessive weight penalty, and research is continuing on development of lightweight, efficient control sound sources.[2]

Noise in ducts has long been considered an attractive application of active noise cancellation because the duct serves as a waveguide both to the source noise and to the control sound. Lueg[3] was issued a patent in the mid-1930s for control of sound in a long duct using a system that consists of a reference microphone to measure the noise to be controlled; a source for the control sound, which is equal in amplitude but opposite in phase with the noise at that point; and a processor that delays to adjust for propagation from the measurement microphone to the control source. A major problem that has delayed implementation of this control concept is the instability that is caused by feedback of the control signal onto the reference microphone. To control this, one research area takes the direction of development of sound sources that are intended to generate sound that propagates in one direction from the control source, thus reducing the feedback.[4] Another direction is to develop a model of the feedback loop in the digital signal processor and subtract the synthesized feedback signal from the measured reference to signal.[5] A third method to control the instability is to eliminate feedback altogether by using a nonacoustic reference, such as the signal from a tachometer on an engine operating at steady state.[6] Utilization of the nonacoustic reference is appropriate when the source noise is periodic, such as is generated by a fan, and when the controller needs only frequency information about the source. The control system described in this paper uses a nonacoustic reference signal from a blade passage sensor on the fan.

Active noise control systems have been shown to reduce multiple harmonic tones of periodic noise generated in a duct by a loudspeaker.[7] Numerous researchers have demonstrated control of duct-borne sound generated by fans, either multiple pure tones[8,9] or broadband fan noise.[5] The results reported generally show the noise reduction at the error microphone where the cancellation is expected to be quite effective. Researchers at Virginia Polytechnic Institute and State University have developed an active control system on the inlet of a commercial jet engine using a ring of loudspeakers as the control source.[10] The error microphones, which are located in the acoustic far field for the experiments with this engine, have a large diaphragm so that the sound is effectively integrated over a finite space. The result is a broadened spatial extent of noise reduction with a slight loss in magnitude. The most significant problem encountered in this experiment is the mode spillover due to mismatch of the mode compositions of the noise and the control sources. This mode spillover results in noise amplification at some locations away from the control microphones.

The purpose of the reported experiment is to develop a control system utilizing error sensors located in the fan duct. It is felt that the spatial extent of noise reduction and, more importantly, the mode spillover effect, can be controlled more effectively with the in-duct error sensor.

Modal Description of Sound Propagation in Ducts

The following discussion summarizes the sound propagation in ducts in terms of discrete modes and the mode generation by rotor/stator interaction. A more complete description of fan noise generation and propagation is given in Appendix A.

A sound wave of radial frequency ω propagating in a duct can be decomposed into circumferential, radial, and axial modes. The radial wave numbers k_{mn} correspond to the n roots of the radial derivative of the m-order Bessel function, evaluated at the duct outer and inner radii. The sound pressure around the circumference of the duct is periodic of the form $\cos(m\theta)$ where m is an integer. Cut-on modes are those modes for which the sound frequency is high enough that the sound wave number $k = \omega/c$ is greater than k_{mn}. Under these

Received Sept. 23, 1995; revision received Sept. 1, 1996; accepted for publication Sept. 30, 1996; also published in *AIAA Journal on Disc*, Volume 2, Number 2.

*Senior Research Engineer, Aeroacoustics Branch, Fluid Mechanics and Acoustics Division, MS 461. Member AIAA.

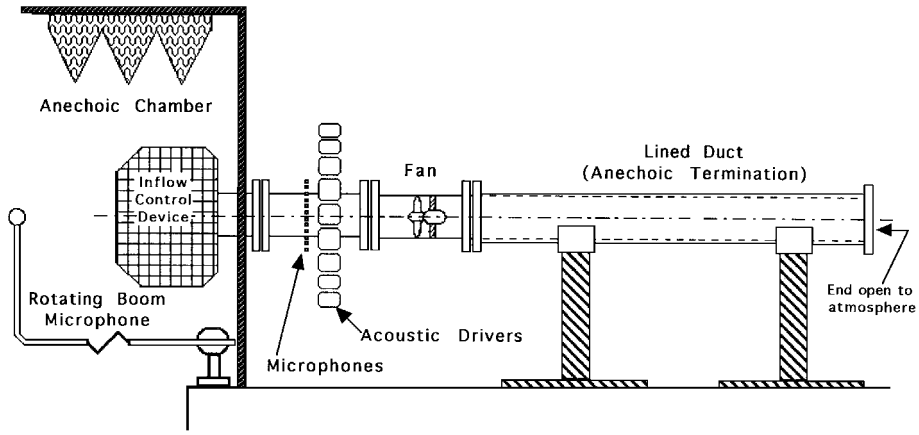

Fig. 1 Fan noise control experiment layout.

conditions the axial wave number is real and sound propagates. The plane wave is always present in the duct since it cuts on at 0 Hz.

The tonal parts of the fan noise occur at the blade passage frequency and its harmonics. The relative number of rotor blades and fan exit guide vanes determine those circumferential modes that are generated at each blade passage frequency harmonic. Only those circumferential modes that result in real axial wave number values can propagate.[11]

Experiment Layout

Duct

The experimental setup consists of a duct with the following major elements: inflow control device, control hardware section, an axial flow fan, and an anechoic termination. The unit is installed in the laboratory space of the Anechoic Noise Research Facility at NASA Langley Research Center. The inlet to the fan duct is in the anechoic chamber, and the remainder of the duct is in the model assembly area adjacent to the chamber. Figure 1 shows a schematic of the overall experiment layout. The anechoic chamber volume is 482 m^3 (17,000 ft^3) and the acoustic wedges on floor, walls, and ceiling are 0.91 m (3 ft) deep, giving a lower cut-off frequency of approximately 100 Hz. Far-field sound measurements are made using a 12.7-mm ($\frac{1}{2}$ in.) B&K microphone on a rotating boom at a radius of 1.52 m (5 ft) from the face of the duct inlet. An inflow control device is installed on the inlet of the duct.[12] The purpose of the inflow control device is to straighten flow into the duct and to break up turbulent eddies, which may be ingested into the fan. The inflow control device is designed to simulate the uniform inflow of forward flight in a static test.[13] Figure 2 is a photograph of the inflow control device on the duct inlet installed in the anechoic chamber. It also shows the far-field microphone.

The control hardware duct piece contains an array of microphones arranged uniformly around the circumference of the duct and installed with sensing surfaces flush with the inside surface of the duct. The microphones are used as the in-duct error sensors for the control system. Although up to 48 microphones can be accommodated in the duct, only two are necessary to determine the plane wave or first-order circumferential modes, and two are used for the present test series. The microphones are 3.2-mm- ($\frac{1}{8}$-in.-) diam electret transducers embedded in a threaded 12.7-mm- ($\frac{1}{2}$-in.-) diam canister. As shown in the photograph (Fig. 3), 12 control drivers are distributed around the duct. Each driver is rated at 120-W rms. The drivers are attached to the duct by transition horns that are thick walled to prevent sound transmission. The horns transition from the round outlet of the driver to the rectangular slot in the duct wall. The areas of both are the same, and so minimum impedance mismatch is expected. A thin wire mesh covers the slot on the inside surface of the duct to reduce cavity resonance as a source of noise. The large number of control sources ensures that higher order modes generated by the discrete number of sources are well above the cut off and thus do not propagate as uncontrolled modes.

The fan, whose outer casing is shown in Fig. 3, is designed to generate noise predominantly by the interaction of the rotor wake

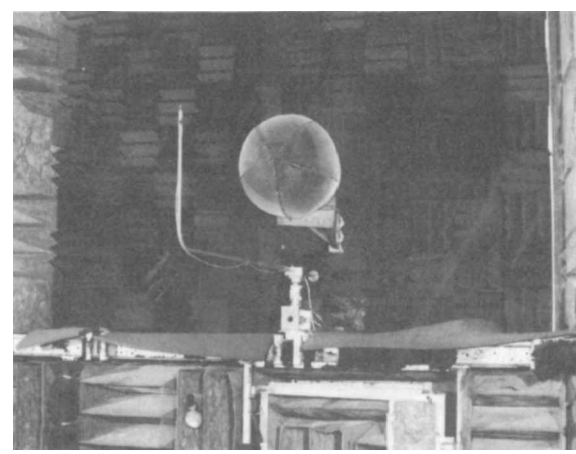

Fig. 2 Fan noise control ductwork: view from inside the anechoic chamber showing inflow control device and far-field microphone.

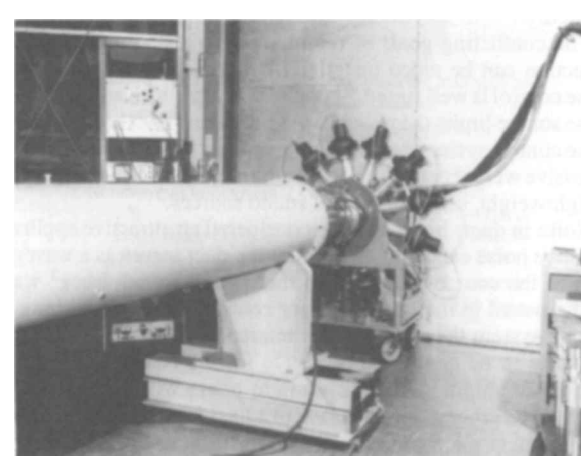

Fig. 3 Fan noise control ductwork: view from outside the anechoic chamber showing noise control hardware, fan, and anechoic termination duct sections.

with the downstream stator. The fan unit consists of a 16-bladed rotor with airfoil-shape blades that are designed to deliver 1.36-kg/s (3 lb/s) airflow and to produce 22.3-N (5-lb) thrust at 4500 rpm. The fan tip diameter is 30 cm (11.81 in.) with a hub diameter of 15.2 cm (6 in.). The fan is driven by a 3-HP electric motor, and rotor speeds up to 6000 rpm can be achieved. The blade passage frequency, thus, can be up to 1600 Hz. The fan has been designed so that the number of stator vanes can be varied and the vane spacing always kept uniform. Predominantly plane waves are generated at blade passage

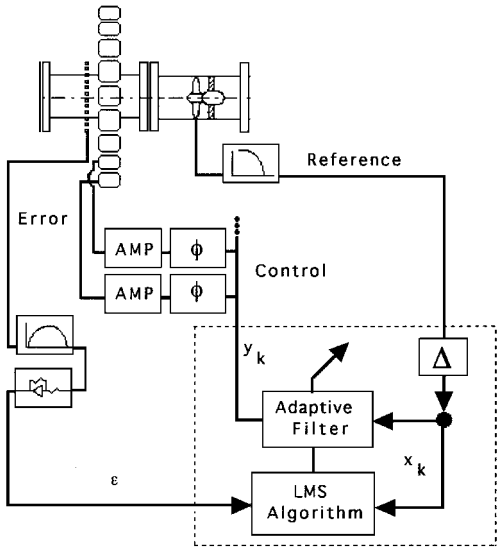

Fig. 4 Fan noise control system setup.

frequency when the fan is configured with 16-stator vanes for the 16-blade rotor, and the first circumferential (spinning) mode will dominate when 17 vanes are installed with the 16-blade rotor. The stator vanes are positioned at 0.5 blade chord length downstream of the rotor to generate a strong rotor/stator tone.

A muffler section is located downstream of the fan, as shown schematically in Fig. 1 and in the photograph, Fig. 3. This 3.7-m-(12-ft-) long duct is lined with perforated metal and 50 mm (2 in.) of sound absorbing material. The muffler reduces fan noise radiation into the laboratory space and, thus, reduces flanking noise. It also acts as an anechoic termination for the discharge of the fan.

Control System

The purpose of the control system is to introduce a mirror image of the fan noise into the duct such that the combined noise from the fan and the control source is a minimum at the error microphone location. It is expected that minimizing the noise within the duct will also reduce the noise radiated from the duct. The control algorithm consists of a four-coefficient adaptive filter, which applies the weighting factor to the reference signal to generate the control signal. The purpose of this project is to demonstrate control of the fan tone noise, so that the reference signal is a tone that is generated at the blade passage frequency of the fan. A least mean square (LMS) algorithm updates the weighting coefficients using the current values of the coefficients and the error, which is the sum of the fan noise and the control signal at the error sensor. The weight coefficient vector is an approximation of the optimum Weiner weight vector. The theory of operation of the control algorithm is discussed in detail in Appendix B.

Figure 4 shows the schematic diagram of the control system, which includes the fan and control hardware sections of the duct. The reference signal for the controller is supplied by a proximity probe, which gives a pulse at each blade passage. The probe signal is low-pass filtered to remove the harmonics of the blade passage frequency leaving a tone at the blade passage frequency, which is input to the computer. The error signal is the combination of the fan and control noise measured at the error microphones. The signal is bandpass filtered, to remove extraneous noise, and amplified before passing into the computer. The output from the computer is the control signal, which is passed through up to 12 channels of gain/phase network to adjust the magnitude and phase of the signal to the individual loudspeaker to generate the control signal in the circumferential mode for which control is sought.

The controller is a Texas Instruments TMS320C30 (C30) floating point digital signal processor board, which is mounted in a personal computer through the ISA bus. The reference and error signals are input to the computer by a 16-bit analog-to-digital converter with a fourth-order filter to prevent aliasing. The analog-to-digital converter has 153-kHz throughput. The signal is output through a 16-bit digital-to-analog converter with fourth-order filter to reconstruct and smooth the digital signal produced by the C30. The digital-to-analog converter has 667-kHz throughput. The whole active, adaptive control system is driven at the sampling frequency (Δ) of the analog-to-digital converters.

Results

Table 1 shows the fan speeds at which the blade passage frequency tones are expected to cut on in the duct. These cut-on values were calculated using the expressions developed in Appendix A with hub-to-tip ratio of 0.5. The table shows that three circumferential modes, each at the lowest radial order, are expected to be cut on at the blade passage frequency when the fan is run at maximum speed. The values in the column with heading *ka* are the wave number normalized by duct outer radius at which cut on is expected to occur.

Plane Wave Generated in the Duct

A series of tests was run with the active, adaptive noise control system incorporated into the fan duct system. The number of stator vanes in the fan is 16 for these tests to excite predominantly plane waves. The signals from two microphones on opposite circumferential locations in the duct are added in phase to measure the error. The 12 control speakers are activated in phase to simulate the plane wave.

Figure 5 shows the directivity plot of fan noise in the acoustic far field with the fan operating at 2350 rpm. The blade passage frequency at this fan speed is 627 Hz, and the normalized wave number *ka* is 1.76. This blade passage frequency is near the first spinning mode cut on. The microphone signal has been filtered so that the directivity plot in Fig. 5 shows the blade passage frequency tone. When the controller is not activated, the directivity plot shows sound radiation that is spatially uniform, confirming the expected plane wave sound propagation in the duct. When the controller is activated, the curves in the figure indicate that the sound level is reduced approximately 14 dB in the far field for observer locations from 0 to 90 deg. This noise reduction was found to be quite stable throughout the time that it took to complete the directivity sweep.

The fan was then run at 2800 rpm, which corresponds to blade passage frequency of 750 Hz, or normalized wave number $ka = 2.10$. This frequency is well above the first spinning mode cut-on

Table 1 Estimated and measured cut on fan speed of modes in the 12-in.-diam duct with 50% hub-to-tip ratio

		Fan speed, rpm	
Mode	*ka*	Estimated	Measured
1,0	1.355	1855	2300
2,0	2.681	3671	3700
3,0	3.958	5420	4800

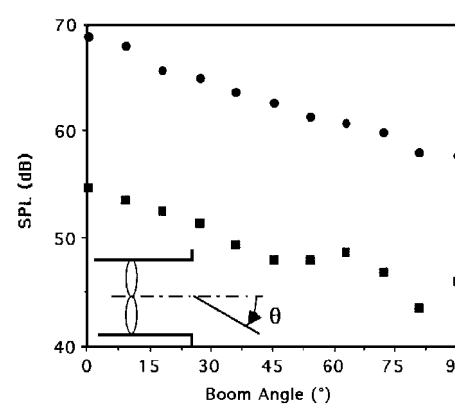

Fig. 5 Far-field directivity of blade passage frequency tone at fan speed 2350 rpm, plane wave dominant: ● control off and ■, control on.

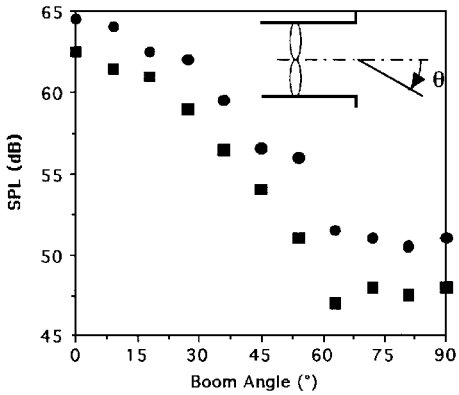

Fig. 6 Far-field directivity of blade passage frequency tone at fan speed 2800 rpm, plane wave dominant: ● control off and ■, control on.

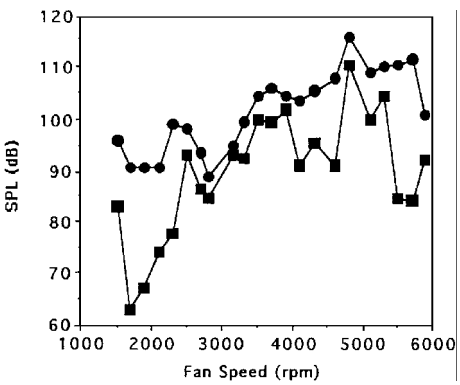

Fig. 7 Sound level spectrum of fan blade passage frequency tone at in-duct error microphone: ● control off and ■, control on.

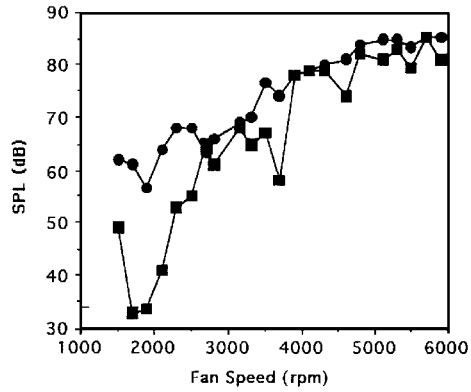

Fig. 8 Sound level spectrum of fan blade passage frequency tone at far-field microphone fixed on the duct axis, $\theta = 0$ deg: ● control off and ■, control on.

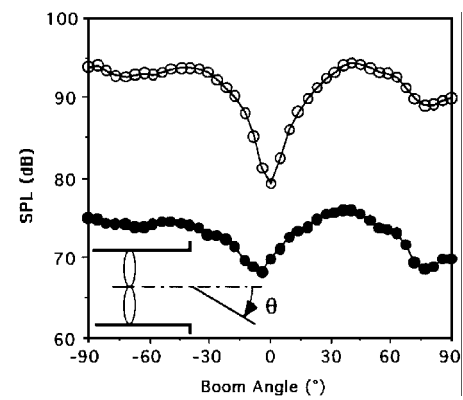

Fig. 9 Comparison of fan blade passage frequency tone to simulation in the far field, fan speed at 2800 rpm, $m = 1$ mode dominant: ○ simulation and ● the fan tone.

frequency for the duct, but it is expected that the spinning mode would not be cut on strongly in light of the fact that the number of blades and stators is the same. This is seen in the directivity plots of the blade passage frequency tones for control off and control on that are shown in Fig. 6. The far-field sound is not as uniform spatially as it was nearer the mode cut on (Fig. 5). However, the sound deficit on the fan axis that is characteristic of the spinning mode dominance is not found in the radiation pattern in Fig. 6, which indicates plane wave dominance. When the controller is activated, the sound level reduction is relatively uniform at 2 dB in the acoustic far field at locations from the fan axis to 90 deg. The far-field noise reduction, while stable and spatially uniform, is much less than it is when blade passage frequency is closer to the spinning mode cut on.

The performance of the controller as a function of frequency is indicated in Fig. 7. This plot was generated by operating the fan at speeds ranging from 500 to 6000 rpm and comparing the blade passage frequency tones at one of the error microphones for control off with control on at each speed. The control-off spectrum for the in-duct error microphone shows a general trend in sound level to go up with engine speed punctuated by increases at 2300, 3700, and 4800 rpm. The increases are due to standing waves in the duct, which are indicative of mode cut on. Comparison of these observed cut-on frequencies with the estimated cut-on frequencies in Table 1 indicates that the second and third circumferential modes show fairly good agreement. The observed first mode cut-on 2300-rpm speed is considerably higher than the estimated speed, and is close to the cut-on speed that would occur with no centerbody correction (2518 rpm).

When the controller is activated, the system reaches steady state with the error microphone signal decreased at all operating speeds. The noise reduction is from 3 dB to as much as 27 dB at the error microphone.

Figure 8 shows the spectral noise reduction achieved in the far field on the axis of the duct. When the control is off, the far-field spectrum is smoother than it is in the duct, showing that the duct standing waves are not propagated into the far field. Noise reduction is obtained with the controller at all operating speeds except in the vicinity of those fan speeds at which the in-duct error microphones registered standing waves in the duct. Comparison of Figs. 7 and 8 shows that the noise reduction in the far field is generally less than that indicated by the in-duct error microphones. In fact, the error microphone signal indicates noise reduction at the critical speeds at which the sound level in the far field is either not affected or is increased.

Spinning Mode Generated in the Duct

A test series was run in which 17 fan exit guide vanes are installed into the fan duct, while the rotor blade count of 16 is retained. It is expected that the difference in the number of vanes and rotor blades will cause the $m = 1$ spinning mode to be excited. The outputs from two microphones mounted on opposite circumferential locations in the duct are added out-of-phase to give the error signal. The out-of-phase addition eliminates any plane wave residual in the signal. The phase of the signal to each of the 12 control loudspeakers is shifted by 30 deg relative to the previous driver to simulate the $m = 1$ mode.

The fan was operated at 2800 rpm, the speed that produces normalized wave number $ka = 2.10$. This is above the first spinning mode cut on, and it is expected that the $m = 1$ spinning mode will be excited into dominance. This is shown in the far-field radiation pattern, the lower curve in Fig. 9. The deficit on the fan axis is indicative of a circumferential mode. The peak of the directivity lobe occurs at approximately 45 deg from the fan axis. The location of the directivity pattern peak Ψ is estimated from[14]

$$\sin\Psi = 1/\zeta$$

where ζ is the cutoff ratio $= ka/(ka)_{\text{cutoff}}$. The peak is estimated to be at $\Psi = 40.2$ deg.

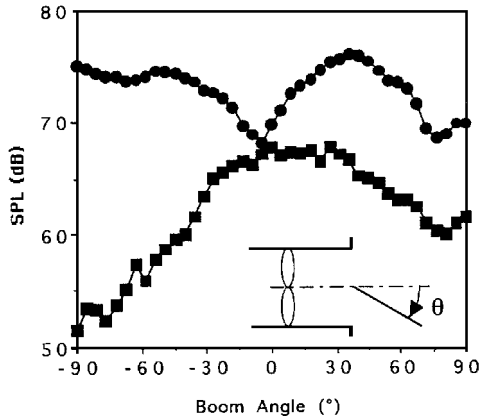

Fig. 10 Far-field directivity of blade passage frequency tone at fan speed 2800 rpm, $m = 1$ mode dominant: ● control off and ■, control on.

The upper curve in Fig. 9 shows directivity of the experimental simulation produced by the control drivers at 750 Hz. The far-field radiation pattern generated by the control drivers is seen to be comparable to the fan noise radiation.

The result of activating the control system is shown in Fig. 10. The spinning mode is virtually eliminated, leaving a radiation pattern that suggests a plane wave. This is reasonable because the plane wave is always generated by the fan and the control system is not programmed to reduce it.

Conclusions

The experiments discussed have verified that time domain active, adaptive control is applicable to reduction of fan noise in a duct. The control system has been applied to tones that are generated at the blade passage frequency. The controller is stable over a range of frequencies in which plane waves and higher-order duct modes can propagate. The system utilizes in-duct error sensing, which is shown to provide global noise reduction in the acoustic far field.

The system is most effective when the mode structures of the noise source and of the control source are the same. When the fan is configured with equal numbers of rotor blades and stator vanes, and the control drivers are configured to generate plane waves, far-field noise reduction is greatest below cut on of higher-order modes. The presence of higher-order modes, even though the plane wave is dominant, compromises noise reduction performance. When the number of stator vanes and rotor blades differs by 1, and the control drivers are programmed to generate the $m = 1$ mode, the control system reduces the first spinning mode, leaving the plane wave component, which is still generated by the rotor/stator interaction. The in-duct error sensor produces a stable control signal, which does not excite uncontrolled higher-order modes.

Generally, the noise reduction measured by the in-duct error sensors is greater than the noise reduction in the far field. Fan operating conditions were found at which the in-duct error sensor indicated noise reduction but no noise reduction was measured in the far field. In some instances the sound in the far field was increased with the control system activated, even though the control system stabilized at significant noise reduction at the error microphone. These conditions occurred when standing waves were present in the duct. This condition is felt to be due to the fact that the control system is reducing the (dominant) standing wave component of the sound while not affecting the propagating component. The discrepancy between the in-duct error sensor performance indication and the far-field noise reduction is the subject of continued research.

Appendix A: Sound Propagation in Ducts and Sound Generation by Rotor/Stator Interaction

The homogeneous wave equation for sound pressure of frequency ω traveling in a cylindrical duct in quiescent medium is solved to define the natural frequencies and mode shapes,

$$\frac{1}{r}\frac{\partial}{\partial r}\left(r\frac{\partial p}{\partial r}\right) + \frac{1}{r^2}\frac{\partial^2 p}{\partial \theta^2} + \frac{\partial^2 p}{\partial z^2} + k^2 p = 0 \qquad \text{(A1)}$$

where

$k = \omega/c$
c = speed of sound
r = radial coordinate
z = axial coordinate
θ = circumferential coordinate

The solution of the wave equation has the general form

$$p(r, \theta, z) = e^{ik_z z} A_m \{J_m(k_{mn} r) + i Q_m Y_m(k_{mn} r)\} \cos(m\theta) \qquad \text{(A2)}$$

The circumferential term $\cos(m\theta)$ satisfies the boundary condition that the sound pressure at angle θ must be the same as the sound pressure at $\theta + 2\pi$. The coefficient m defines the order of the circumferential or spinning mode.

The radial term consists of Bessel functions of the first and second kind. The radial wave numbers k_{mn} are evaluated from the n zeros of the derivatives of the Bessel functions associated with the mth circumferential mode. The terms come from the boundary condition of zero radial velocity at the duct outer wall and inner hub. The radial velocity is proportional to the radial derivative of the pressure, so that

$$v_r(r_{\text{out}}, \theta, z) = 0 \Rightarrow \left(\frac{\partial J_m}{\partial r} + Q_m \frac{\partial Y_m}{\partial r}\right)\bigg|_{r = r_{\text{out}}} = 0 \qquad \text{(A3a)}$$

and

$$v_r(r_{\text{in}}, \theta, z) = 0 \Rightarrow \left(\frac{\partial J_m}{\partial r} + Q_m \frac{\partial Y_m}{\partial r}\right)\bigg|_{r = r_{\text{in}}} = 0 \qquad \text{(A3b)}$$

Expressions (A3a) and (A3b) are solved simultaneously for the roots, k_{mn}, and the shape factor term Q_m.

The axial wave number is evaluated from the relationship

$$k_z = \sqrt{k^2 - k_{mn}^2} \qquad \text{(A4)}$$

When the sound frequency is high enough that the wave number k is greater than the wave number of the nth radial mode associated with the mth circumferential mode, k_z is real and sound propagates. The m, n mode, thus, is said to be cut on. For low frequencies such that $k < k_{mn}$, k_z is imaginary. The argument of the exponential term in Eq. (A2) is real and negative indicating that the sound pressure decays as it moves down the duct. The modes for which $k < k_{mn}$ are said to be cut off.

Table 1 shows the cut-on wave numbers for modes in the 12-in.-diam duct. The number of modes that can propagate in the duct at the blade passage frequency is three for fan speeds up to the maximum of 6000 rpm. The cut-on frequencies are calculated from simultaneous solution of Eqs. (A3a) and (A3b), using hub-to-tip ratio, $r_{\text{in}}/r_{\text{out}}$, of 0.5. The wave numbers in the table are normalized by the duct outer radius $r_{\text{out}} = a$.

The tonal part of the fan noise is generated by the impingement of the vortices shed from the rotor on the downstream fan exit guide vanes. These tones occur at the blade passage frequency and its harmonics. When the frequency is high enough that the wave can propagate, the fan tones travel in spinning modes defined from the relationship[11]

$$m = n_h B + kV \qquad \text{(A5)}$$

where

n_h = harmonic number
B = number of blades
V = number of fan exit guide vanes
k = any positive or negative integer, including zero

Although an infinite number of circumferential modes can be generated by rotor/stator interaction, only those modes for which the axial wave number is real, from Eq. (A4), will propagate. When the number of blades and the number of vanes is the same, the plane wave $m = 0$ is most strongly excited. When the difference in the number of blades and vanes is 1, the first spinning mode will dominate at frequencies above the $m = 1$ cut on. The spinning mode is characterized by a sound radiation deficit on the fan axis.

The sound is in a lobe, which radiates perpendicular to the duct axis when the mode is first cut on and progresses toward the duct axis as the frequency increases.[15]

Appendix B: Control Theory

This section discusses the general theoretical development of the LMS algorithm and the adaptive filter. The generalized control system consists of a plant in which some measurable continuous signal s is the input and the output is a disturbance signal d. The control system generates a discretized signal y_k, which combines with the disturbance to produce an error ε. It is the purpose of the control system to generate the signal that minimizes the error.

The continuous signal s is sampled at discrete time intervals Δ in the digital computer and collected into a vector $\boldsymbol{X}_k$ of length n,

$$\boldsymbol{X}_k = \begin{Bmatrix} x_k \\ x_{k-1} \\ \vdots \\ x_{k-n+1} \end{Bmatrix} \tag{B1}$$

The element x_k is the digitized sample of s taken at the present time. The element x_{k-1} is the digitized sample of s taken on the previous loop, Δ in the past, and so on to x_{k-n+1}, which is the digitized sample of s taken $(n-1)*\Delta$ in the past. The vector $\boldsymbol{X}_k$ is constantly updated on each loop with the oldest value discarded and the newest value put in the top of the array. The scalar output of the adaptive filter is obtained from

$$y_k = \sum_{l=0}^{n-1} w_l x_{k-l} = \boldsymbol{W}^T \boldsymbol{X}_k \tag{B2}$$

where

$\boldsymbol{W}^T$ = transpose of the vector $\boldsymbol{W}$
$\boldsymbol{W}$ = vector of weighting coefficients

$$\boldsymbol{W} = \begin{Bmatrix} w_0 \\ w_1 \\ \vdots \\ w_{n-1} \end{Bmatrix}$$

The error at time t_k is the combination of the disturbance and the filter output

$$\varepsilon = d - \boldsymbol{W}^T \boldsymbol{X}_k \tag{B3}$$

The mean square error ε^2 is minimized by setting to zero the derivative of the expectation of the mean square error with respect to the weighting vector.[16] The LMS algorithm is intended to approximate the optimum solution in real time, using the method of steepest descent. The weight function for the current loop through the controller $\boldsymbol{W}_j$ is updated using the weight function from the previous pass through the loop $\boldsymbol{W}_{j-1}$ plus a change proportional to the negative gradient of the mean square error ∇_j

$$\nabla_j = \begin{Bmatrix} \dfrac{\partial(\varepsilon_k^2)}{\partial w_0} \\ \vdots \\ \dfrac{\partial(\varepsilon_k^2)}{\partial w_{n-1}} \end{Bmatrix} = 2\varepsilon_k \begin{Bmatrix} \dfrac{\partial(\varepsilon_k)}{\partial w_0} \\ \vdots \\ \dfrac{\partial(\varepsilon_k)}{\partial w_{n-1}} \end{Bmatrix} \tag{B4}$$

where ε_k is the current value of the digitized sample of the error.

The slope of the error curve is evaluated from expression (B3):

$$\begin{Bmatrix} \dfrac{\partial(\varepsilon_k)}{\partial w_0} \\ \vdots \\ \dfrac{\partial(\varepsilon_k)}{\partial w_{n-1}} \end{Bmatrix} = \boldsymbol{X}_k \tag{B5}$$

The weighting vector is updated in the LMS algorithm according to the expression

$$\begin{aligned} \boldsymbol{W}_j &= \boldsymbol{W}_{j-1} - 2\mu\nabla_j \\ &= \boldsymbol{W}_{j-1} - 2\mu\varepsilon_k \boldsymbol{X}_k \end{aligned} \tag{B6}$$

where μ is the user-defined adaptation constant.

The algorithm will converge in the mean and will be stable as long as the adaptation constant μ is positive and less than the reciprocal of the largest eigenvalue of the matrix formed from the product of the vector $\boldsymbol{X}_k$ and its transpose.[16] The speed with which the algorithm converges is dependent on the adaptation coefficient, and the convergence is greatest for the largest value of μ that does not violate the maximum value criterion. The expected value of the weight vector in expression (B6) converges to the optimum Weiner weight vector when the input vectors are uncorrelated over time.

References

[1]Chaplin, G. B., "Anti-Noise, the Essex Breakthrough," *Chartered Mechanical Engineer*, Vol. 30, Jan. 1983, pp. 41–47.

[2]Dungan, M. E., "Development of a Compact Sound Source for the Active Control of Turbofan Inlet Noise," M.S. Thesis, Mechanical Engineering Dept., Virginia Polytechnic Inst. and State Univ., Blacksburg, VA, June 1992.

[3]Lueg, P., "Process of Silencing Sound Oscillations," U.S. Patent 2,043,416, 1936.

[4]Swinbanks, M. A., "The Active Control of Sound Propagation in Long Ducts," *Journal of Sound and Vibration*, Vol. 27, No. 3, 1973, pp. 411–436.

[5]Eriksson, L. J., Allie, M. C., Bremigan, C. D., and Gilbert, J. A., "Active Noise Control on Systems with Time-Varying Sources and Parameters," *Sound and Vibration*, Vol. 23, No. 7, 1989, pp. 16–21.

[6]Eghtesadi, K., and Chaplin, G. B., "The Cancellation of Repetitive Noise and Vibration by Active Methods," *Proceedings of NOISE-CON '87* (State College, PA), Noise Control Foundation, New York, 1987, pp. 347–352.

[7]Tichy, J., Warnacha, G. E., and Pool, L. A., "Active Noise Reduction Systems in Ducts," ASME Paper 84-WA/NCA-15, Nov. 1984.

[8]Ffowcs Williams, J. E., "The Silent Noise of a Gas Turbine," *Spectrum*, Vol. 175, No. 1, 1981.

[9]Koopman, G. H., Fox, D. J., and Niese, W., "Active Source Cancellation of the Blade Tone Fundamental and Harmonics in Centrifugal Fans," *Journal of Sound and Vibration*, Vol. 126, No. 2, 1988, pp. 209–220.

[10]Thomas, R. H., Burdisso, R. A., Fuller, C. R., and O'Brien, W. F., "Active Control of Fan Noise from a Turbofan Engine," AIAA Paper 93-0597, Oct. 1993.

[11]Tyler, J. M., and Sofrin, T. G., "Axial Flow Compressor Noise Studies," *SAE Transactions*, Vol. 70, 1962, pp. 309–332.

[12]Homyak, L., McArdle, J. G., and Heidelberg, L. J., "A Compact Inflow Control Device for Simulating Flight Fan Noise," AIAA Paper 83-0680, June 1983.

[13]Chestnutt, D. (ed.), *Flight Effects of Fan Noise*, NASA CP-2242, Jan. 1982.

[14]Rice, E. J., "Multimodal Far-Field Acoustic Radiation Using Mode Cutoff Ratio," *AIAA Journal*, Vol. 16, No. 9, 1978, pp. 906–911.

[15]Rice, E. J., and Heidmann, M. F., "Modal Propagation Angles in a Cylindrical Duct with Flow and Their Relation to Sound Radiation," AIAA Paper 79-0183, Jan. 1979.

[16]Widrow, B., Glover, J. R., McCool, J. M., Kaunitz, J., Williams, C. S., Hearn, R. H., Zeidler, J. R., Dong, E., and Goodlin, R. C., "Adaptive Noise Canceling: Principles and Applications," *Proceedings of the IEEE*, Vol. 63, No. 12, 1975, pp. 1692–1716.